Secure practical indoor optical wireless communications using quantum key distribution

Vincent Lee[1] and Dominic O'Brien[1]

[1]Department of Engineering Science, University of Oxford, Oxford, UK

***Abstract*—Quantum Key Distribution (QKD) can guarantee security for practical indoor optical wireless environments. The key challenges are to mitigate artificial lighting and ambient light at the receiver. A new spectral region for QKD is proposed and an ideal QKD link model is simulated with experimental ambient light power measurements. Simulation, modelling, and analysis indicates that the carbon dioxide and water absorption band (1370 nm) is a new wavelength region for QKD operation in indoor optical wireless environments. For a feasible QKD link, approximately 20 dB of signal to noise ratio (SNR) is required and a maximum quantum bit error rate (QBER) of 11% when using the BB84 protocol. Links in the new spectral region with a FOV of several degrees are feasible, depending on available components.**

***Index Terms*—Absorption band, ambient light, BB84, carbon dioxide, indoor, optical, QBER, QKD, simulation, SNR, spectrum, water, wireless.**

I. Introduction

Privacy is still a major concern in the digital information era. Quantum communications uses quantum mechanics and the physical properties of light to guarantee security. One practical application to ensure privacy and security is Quantum Key Distribution (QKD). QKD allows the secure distribution of encryption keys and offers enhanced physical layer security with eavesdropper detection to guarantee security.

QKD has been demonstrated for long distance optical communications, terrestrial and free space, but not in indoor optical wireless environments. The key challenges to implement an indoor free space QKD link are mitigating artificial lighting and ambient light at the receiver. Ambient light and light from LEDs are sources of illumination in a typical office room environment, and hence interference. Ambient light from the sun is the main cause of noise in the QKD link.

II. Scenario

Fig 1 shows a typical office room environment with a line of sight (LOS) QKD link with a transmitter (Tx) on the ceiling and a receiver (Rx) on the floor with half angle field of view (FOV). An indoor QKD link is modelled, with a LED point source for artificial lighting and a window allowing sunlight to illuminate the room. The following assumptions are used:

- The QKD link consists of one transmitter on the ceiling and one receiver on the floor
- The transmitter and receiver can track each other
- The transmitter and receiver utilize beamsteering techniques to always point directly at each other and single photons arrive incident at receiver
- The LED is a Lambertian source and the artificial lighting is suitable for a reading environment (average 500 lux across the floor)
- Sunlight illuminates within the room and incident on the receiver

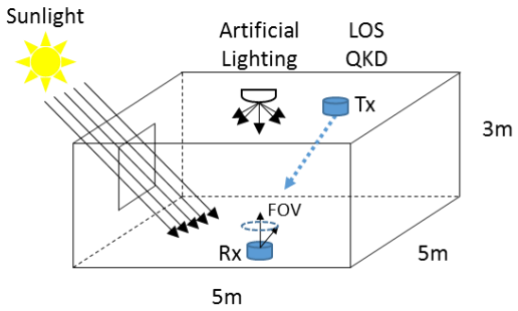

Fig 1. Typical office environment

A. *LED Model*

Artificial lighting from a typical LED light bulb (Cree LED BR30 Flood Light) is modelled. The LED has parameters shown in Table 1 with an emission spectrum (Fig. *2*). The light source is modelled as a point source located at the center of the ceiling at a height of 3 meters off the floor. The LED is a Lambertian source with 60 degrees half power semi angle (Lambertian order m=1) to distribute the light to the edges of the room.

Cree LED BR30 Flood Light (1 Bulb)	
Color temperature	2700 K (Soft-White)
Electrical power (Watts)	9.5
Brightness (Lumens)	650
Optical power (Watts)	0.95

Table 1: Typical LED light bulb emission parameters

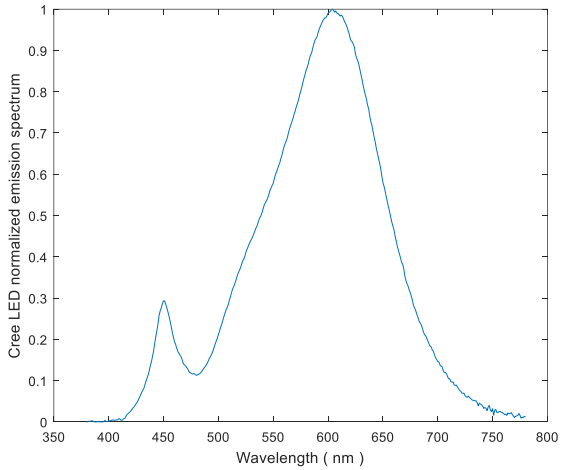

Fig. 2. Cree LED normalized emission spectrum vs wavelength

The output power of the point source is equivalent to 6 bulbs, approximately 6W optical power, to sufficiently illuminate the room with average intensity 500 lux across the floor.

B. *Ambient Light Model*

Sunlight is modelled using measured spectral irradiance of sunlight at sea level (air mass 1.5) with reasonable cloudless atmospheric conditions [1]. Fig. *3* shows the measured spectral irradiance with 2π steradian field of view.

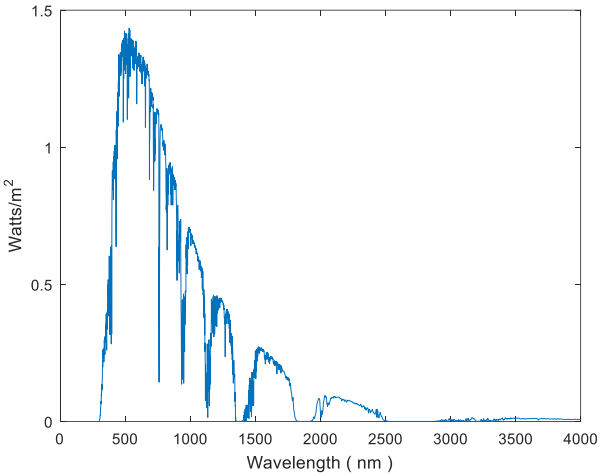

Fig. 3. ASTM measured spectral irradiance vs wavelength [1]

III. Key Mitigation Parameters

Key mitigation parameters such as timing window, wavelength filtering, and spatial filtering are necessary to reduce the ambient light onto the receiver. The timing window is a period when the receiver expects a QKD signal to arrive. The receiver should operate within a relatively short timing window to limit the exposure to ambient light and reduce the probability of more photons. The wavelength filtering defines the spectral region of interest where the receiver rejects any signal outside of this region. The receiver should use a narrowband filter to reduce the spectral power of ambient light. The spatial filtering such as field of view and collection area can further limit the ambient light at the receiver. The field of view is the maximum viewing angle for the receiver and only light that enters within the angle can pass through to the detector. The receiver should have a narrow field of view to limit the light entering onto the detector. The collection area is the size of the photo detector's active area in the receiver. The receiver should have a small collection area to limit the ambient light incident on the active area.

Experiments of free space optical QKD utilizing these key mitigation parameters have been conducted [2] [3] [4] [5] [6] [7] [8]. Examples of key mitigation parameters to improve the single photon detection include the receiver operating within a timing window of 1 nanosecond, a narrowband filter of 1 nm, a field of view of 0.1°, and a collection area of 5 mm^2.

IV. Signal To Noise Ratio

The standard metric used to quantify a communications link is signal to noise ratio (SNR). For a feasible QKD link, approximately 20 dB of SNR is required [2] [9]. The SNR is given by

$$SNR_{dB} = 10log_{10}\left[\frac{P_R}{P_N}\right] \tag{3}$$

where P_R is received power at the detector and P_N is the noise power at the detector.

The standard QKD metric to detect an eavesdropper is the quantum bit error rate (QBER). QBER is calculated as a ratio of the total number of errors to the total number of received photons and displayed as a percentage [10]. Each QKD protocol has a QBER threshold. The first and simplest to implement QKD protocol is BB84 [11] where polarization bases are used for the quantum channel. A common threshold for the BB84 protocol is 11% [12] [13]. In this simulation, the QBER thresholds are marked as 1% = 20 dB, 4% = 14 dB, and 10% = 10 dB [10].

Noise power at the detector mainly consists of ambient light. However, in BB84, the quantum key depends on how accurately the photon maintains its polarization state at the output of the 50:50 beamsplitter. Once the photon reaches a detector, there is a probability the state will contribute noise. Hence, noise power based on polarizer misalignment at the detector is also considered. The assumption is the received power contributes 1% noise power due to polarization misalignment (P_{pol}) [10].

The SNR is therefore modified, and given by

$$SNR_{dB} = 10log_{10}\left[\frac{P_R}{P_{pol} + P_{R\_amb}}\right] \quad (4)$$

where P_R is received power at the detector, P_{pol} is the noise power due to polarization misalignment, and P_{R_amb} is the filtered ambient light power at the receiver.

V. 1370 NM SPECTRAL REGION

Data from the solar spectrum [1] shows there is significantly lower ambient light noise in the water and carbon dioxide absorption band [14] between 1360 – 1370 nm. This was therefore identified as a promising region in which to operate an indoor QKD link, and investigation into the solar spectrum in the 1360 – 1370 nm region was undertaken.

A. LED Mitigation

The primary focus on the LED emission spectrum is the use of commercial, silicon-based photo detectors such as Silicon Avalanche Photo Diodes (Si APDs) and Single Photon Avalanche Diodes (SPADs) for single photon detection. The silicon detection spectrum ranges from 300 – 1100 nm and, particularly between 600 – 1000 nm, Si APDs are nearly 100% quantum efficient with anti-reflection coatings [15]. Commercial Si APDs and SPADs can detect with up to 85% quantum efficiency in the visible light spectrum [16] [17] [18] [19]. For the QKD link model, artificial lighting contributes minimal noise because the LED does not emit in the 1370 nm region.

VI. 1370 NM QKD LINK MODEL

In order to quantify the potential signal to noise ratio (SNR) benefit of operating at 1370 nm, a link model was developed and the results of a link simulation are reported in this paper. Fig. *4* shows the model.

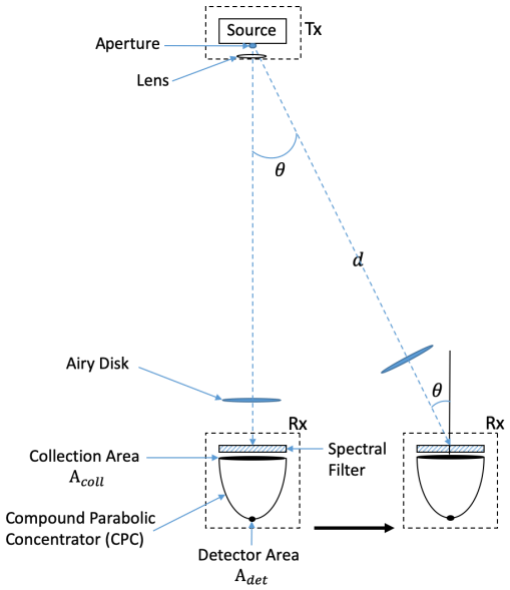

Fig. 4. Free space link diagram

The transmitter (Tx) is a 1370 nm source that can output the minimum required power necessary for single photon transmission to the receiver. The receiver (Rx) has the ability to detect single photons at 1370 nm in the presence of ambient light. The receiver uses ambient light spectral filtering and a compound parabolic concentrator (CPC) to increase the detection of transmitted single photons. It is assumed the transmitter and receiver can track each other using beamsteering techniques. The receiver is placed at a distance d at every half angle FOV θ with respect to the normal of the Rx.

A. Transmitter

The transmitter (Tx) consists of a source with an aperture and lens. The transmitter focuses enough power from a flat wavefront through an aperture and lens to create an Airy disk at the focal length of the lens [20]. In the model, the focal length is equal to distance d. The power within the Airy disk is equal to the minimum power necessary for single photon transmission. The size of the Airy disk is given by

$$\emptyset \mathrm{A} = \frac{2.44\lambda_0 d}{\emptyset S} \tag{5}$$

where λ_0 is transmit wavelength, d is distance, $\emptyset$A and $\emptyset S$ are the circular diameters of the Airy disk and source's aperture respectively.

B. Receiver

The receiver (Rx) consists of a spectral filter, compound parabolic concentrator (CPC), and flat photodetector.

1) Spectral filter

The spectral filter is an interference filter used to filter the ambient light and allow a narrow range of wavelengths to be transmitted to the detector. The spectral filter has a spectral transmittance (F_T) at a central filter wavelength longer than the transmit wavelength λ_0. The spectral filter passband shifts to shorter wavelengths when the half angle FOV θ increases [21]. The wavelength shift is given by

$$\lambda(\theta) = \lambda_0 \sqrt{1 - \left(\frac{\sin\theta}{n_e}\right)^2} \tag{6}$$

where λ_0 is transmit wavelength, θ is half angle FOV, and n_e is the effective refractive index of the spectral filter. Fig. 5 shows the effect of the spectral filter passband shift.

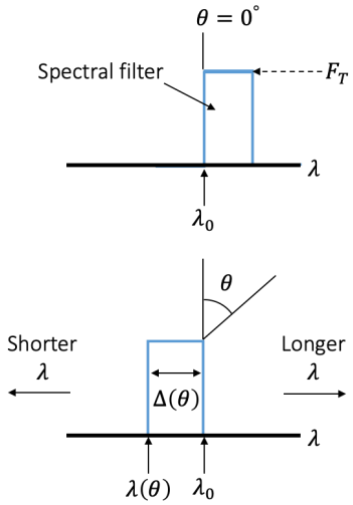

Fig. 5. Spectral filter passband shift

For each half angle FOV θ, a new spectral filter bandwidth $\Delta(\theta)$ must be designed to ensure the transmit wavelength λ_0 remains within the passband, leading to an increase in the optical bandwidth as the FOV of the link is increased.

2) Compound Parabolic Concentrator

The compound parabolic concentrator (CPC) is used to increase the received power detection at the receiver. Fig. 6 shows a CPC coupled to a flat detector.

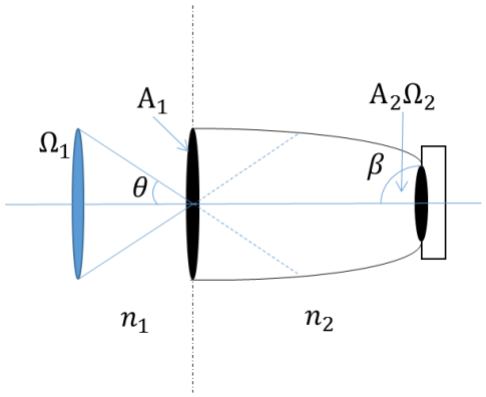

Fig. 6. CPC and flat detector design

The CPC focuses the incoming light from the input diameter of A_1 to the edges of the output diameter of A_2 [22]. One advantage of a CPC is the increased effective collection area A_1 compared to the detector area A_2. In order to calculate the effective collection area of a CPC, etendue must be conserved. Etendue is a "geometric quantity that measures the flux gathering capability of an optical system" [23]. This quantity is conserved, so that

$$A_1\Omega_1 = A_2\Omega_2 \tag{7}$$

where A_1 and A_2 are the areas and Ω_1 and Ω_2 are the solid angles of input and output respectively. Fig. *6* shows that θ is the input acceptance angle, β is the output acceptance angle, n_1 is the refractive index of the input medium, and n_2 is the refractive index of the output medium. Therefore, the effective collection area A_1 is given by

$$A_1 = \frac{(n_2 \sin\beta)^2}{(n_1 \sin\theta)^2} A_2 \tag{8}$$

C. Link

1) Signal

In the QKD link model, the transmitter is a 1370 nm source that can output the minimum required power necessary for single photon transmission to the receiver. In order to achieve single photons, the Poisson probability must satisfy a mean photon number of 0.1 of any repetition rate. This means that sampling 1 out of 10 transmit pulses (0.1 photons per pulse) will ensure an average probability of 1 photon over the sampling period.

2) Noise

The receiver is an optical detector that can detect single photons at 1370 nm. The receiver utilizes a narrow timing window to detect a signal photon and to reduce the ambient light as much as possible.

3) Link Loss

For an indoor free space optical communications link, the received power is proportional to the geometrical loss from the effective collection area and the Airy disk area. Link loss (L_L) can be defined as the ratio of the receiver collection area with respect to the angle of incidence over the Airy disk area.

$$L_L = \begin{cases} 1 \quad , \quad if \quad \dfrac{A_1 \cos\theta}{\frac{\pi}{4}(\emptyset A)^2} \geq 1 \\ \dfrac{A_1 \cos\theta}{\frac{\pi}{4}(\emptyset A)^2} \quad , \quad else \end{cases} \tag{9}$$

where A_1 is the receiver collection area and $\emptyset A$ is the Airy disk circular diameter. In the model, it is assumed the power within the Airy disk is uniform across the flat detector. Hence, if the Airy disk area is within the receiver collection area, then $L_L = 1$ and there is no link loss (0 dB).

D. Ambient Light

Fig. *7* shows the ambient light spectrum data scaled from 100,000 lux to 1,000 lux to simulate ambient light in a typical office room environment. The amount of ambient light detected by the receiver depends on the spectral filter bandwidth and detector etendue.

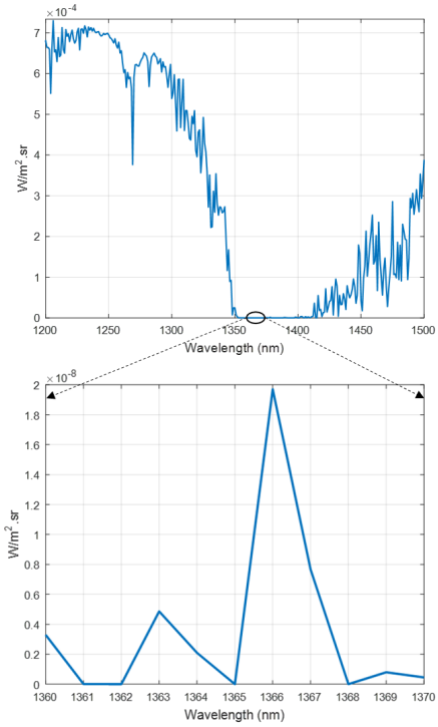

Fig. 7. Ambient light spectrum vs wavelength between 1360-1370 nm

Fig. *8* shows the ambient light modeled as a Lambertian source with intensity profile $m = 1$ with an irradiance angle equal to θ. The concentrator is assumed to be ideal and therefore the etendue of the detector controls the amount of ambient light received. Ambient light enters at up to the maximum acceptance angle of the flat detector ($\beta = 90^{\circ}$). Thus, the ambient light power at the receiver is given by

$$P_{R\_amb} = (m+1)\cos^{m}\theta(\pi(n_2)^2 \mathrm{A}_{det})L_{amb}\cos\theta \quad (10)$$

where n_2 is the refractive index of the CPC, A_{det} is the detector area, and L_{amb} is the filtered ambient light radiance ($Wm^{-2}sr^{-1}$) over a spectral filter bandwidth selected for each half angle FOV θ.

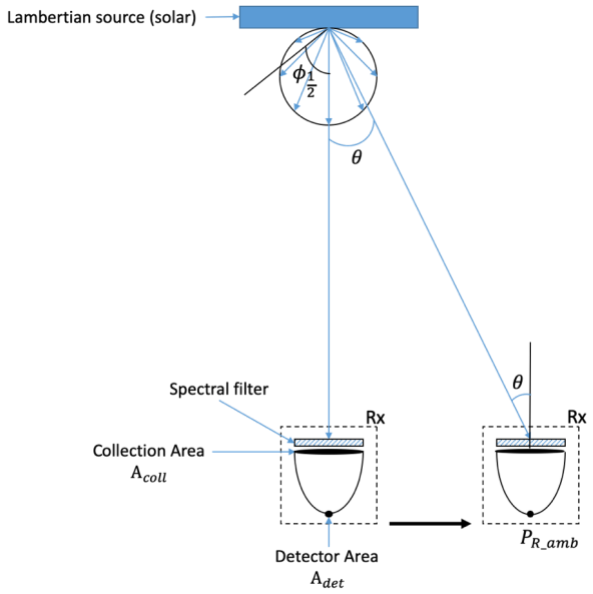

Fig. 8. Ambient light as Lambertian source

VII. 1370 NM QKD LINK SIMULATION

A. *Parameters*

The QKD link model is simulated for a practical office room environment. In the simulation, the transmitter and receiver are separated by a minimum of 3 meters which is the typical height of a room. The transmitter is designed to propagate a beam of light that creates 1 mm, 2 mm, and 4 mm diameter Airy disks at the receiver. A typical detector is a Single Photon Avalanche Detector (SPAD) made by Micro Photon Devices [24]. This SPAD is a $\emptyset 25\mu m$ free space flat detector that can detect a period as low as 150 ps, thus the timing window of 1 ns is a reasonable value for this simulation. The output diameter of the ideal CPC is equal to the $\emptyset 25\mu m$ free space flat detector.

In the QKD link model, the assumption is the transmitter and receiver track each other using beamsteering techniques. Hence, link loss is only dependent on the proportion of the Airy disk illuminating the effective collection area at the receiver. The received power P_R at the detector is given by

$$P_R = (PPS_T)\left(\frac{hc}{\lambda_0}\right)(L_L)(F_T)(\eta)(BS) \tag{11}$$

where h is Planck's constant and c is speed of light.

The received power is attenuated by several parameters at the receiver: spectral filter transmittance (F_T), detector efficiency (η), and the beamsplitter (BS). The spectral filter transmittance is the average transmittance of a commercial (Spectrogon) 10 nm interference filter [25]. The detector efficiency is the maximum efficiency of the commercial (Micro Photon Devices) free space flat detector [24]. A 50:50 beamsplitter is considered due to the typical receiver setup of the BB84 protocol where two orthogonal polarization bases are used [11]. The ambient light spectrum is filtered based on a selected spectral filter bandwidth for each half angle FOV θ. The filtered ambient light power at the receiver P_{R_amb} is calculated using the detector etendue ($A_{det} = \pi(\emptyset 25\mu m)^2/4$ and $\Omega = \pi(1.5)^2$). Fig. *9* shows the filtered ambient light power at the receiver P_{R_amb} across half angle FOV θ.

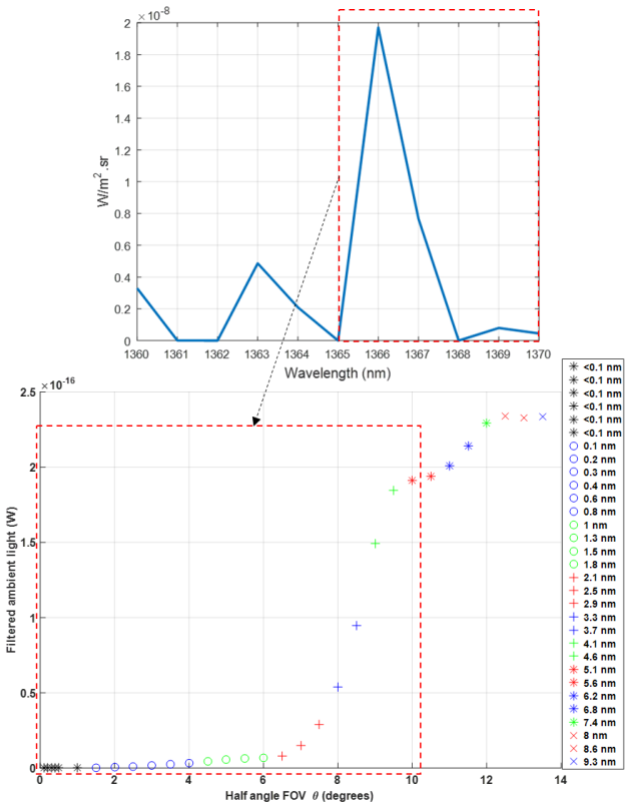

Fig. 9. Filtered ambient light vs half angle FOV

The legend on the right shows the spectral filter bandwidth used for each half angle FOV θ. The ambient light increases slowly for small FOV. Then there is a large increase in the total amount of filtered ambient light as the optical bandwidth of the filter is increased to allow for the passband shift, and the 1366 nm peak of the spectrum is transmitted through the filter. There is then a further slower increase for wider FOVs, and hence optical bandwidths.

B. SNR Estimation

The signal to noise ratio (SNR) is estimated to quantify the simulation with the chosen parameters in Table 2.

Parameter	Value
Transmit signal rate (PPS_T)	100e6 $Photons.s^{-1}$
Transmit wavelength (λ_0)	1370 nm
Spectral filter transmittance (F_T)	0.65
Detector efficiency (η)	0.4
Beamsplitter (BS)	0.5
Detector area (A_{det})	$\pi(\emptyset 25\mu m)^2/4$

Table 2. SNR parameters

Fig. *10* shows the results of the simulation using different Airy disk diameters for SNR across half angle FOV θ. Polarization misalignment dominates the noise term in SNR up to θ = 4 degrees. As θ increases beyond 4 degrees, the filtered ambient light dominates the noise term. Overall, the SNR is high enough for Airy disk diameters of 1, 2, and 4 mm to satisfy a QBER = 10% up to θ = 14 degrees in the presence of ambient light. However, a realistic QBER threshold to satisfy is 4% especially for a mean photon number = 0.1 [10]. Accordingly, the SNR for an Airy

disk diameter of 4 mm is sufficient enough above QBER = 4% when a 4.1 nm spectral filter bandwidth is used. This provides up to 9 degrees half angle FOV θ in the presence of ambient light.

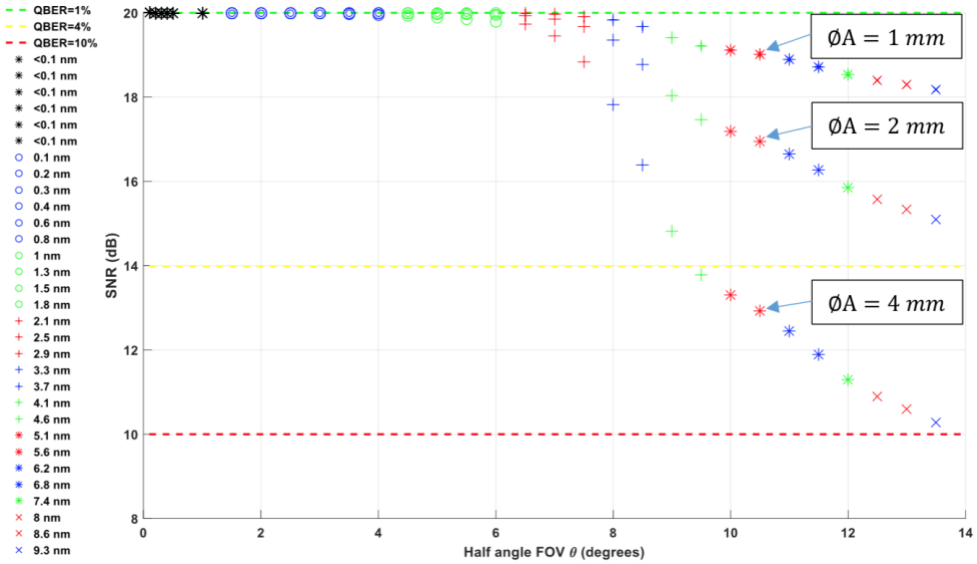

Fig. 10. SNR vs half angle FOV

VIII. Ambient Light And Lambertian Surface Experiment

In order to verify the simulation results, an experiment was undertaken to measure the ambient light from a white wall to simulate a typical indoor room environment. Fig. *11* shows the experimental layout.

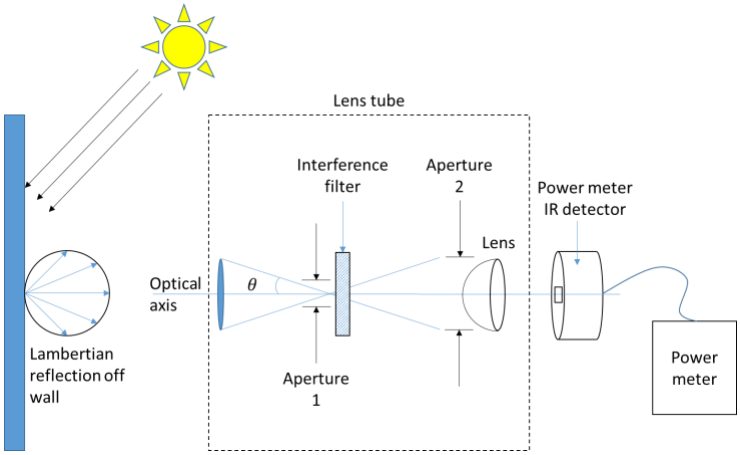

Fig. 11. Lambertian surface ambient light experiment

The measurement equipment consisted of a lens tube and a power meter. The lens tube uses a Spectrogon interference filter centered at 1370 nm with a 10 nm passband [25], two apertures, and a 16 mm focal length lens. The output of the lens tube was connected to a Newport 1830-C power meter and the power meter was used to measure the reflected power off the white wall. The apertures were used independently to control collection area and FOV. Aperture 1 was used to adjust the collection area A_{coll} and aperture 2 was used to adjust the half angle FOV θ. The illumination level was measured using an Amprobe LM-100 lux meter.

Fig. *12* shows the filtered ambient light radiance vs. half angle FOV θ, showing both experimental (red) and the simulated result using the ASTM spectrum (black) data.

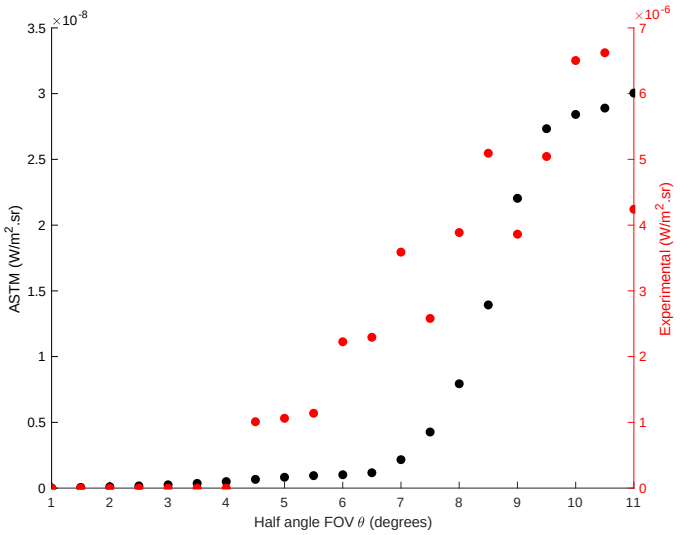

Fig. 12. Filtered ambient light radiance vs half angle FOV

The experimental data was measured from 1 to 11 degrees half angle FOV θ and was normalized to 1000 lux to compare with the simulated ASTM spectrum data. Similar to the filtering method used for Fig. *9*, the experimental data was filtered based on a selected spectral filter bandwidth for each half angle FOV θ.

Measurement results yield experimental data that is several orders of magnitude different from the ASTM spectrum data. The cause for the increase in magnitude for the experimental data is the Spectrogon interference filter does not reduce the light outside of the narrow bandwidth enough. The interference filter has OD3 reduction for all undesired wavelengths while the simulated ASTM spectrum data uses ideal bandwidths with sharp cutoffs outside the region of interest and zero transmittance for all undesired wavelengths. Thus, the power meter measures all wavelengths from 800-1650 nm and the total power measured with the Spectrogon interference filter for all wavelengths outside 1360-1370 nm is of the magnitude e-6.

Fig. *13* shows the SNR curves using the experimental data with different Airy disk diameters. It can be seen that the target SNR can be designed for a half angle FOV θ depending on the Airy disk diameters. The QKD link is feasible for half angle FOV θ less than 4 degrees regardless of Airy disk diameter. Beyond θ = 4 degrees, the size of the Airy disk diameter is an important factor for the feasibility of the QKD link. The QKD link is feasible up to 5.5 degree half angle FOV θ using a 1 mm Airy disk diameter. The QKD link is not feasible using a 2 or 4 mm Airy disk diameter for a target QBER = 4% due to increased link loss and ambient light noise past θ = 4 degrees.

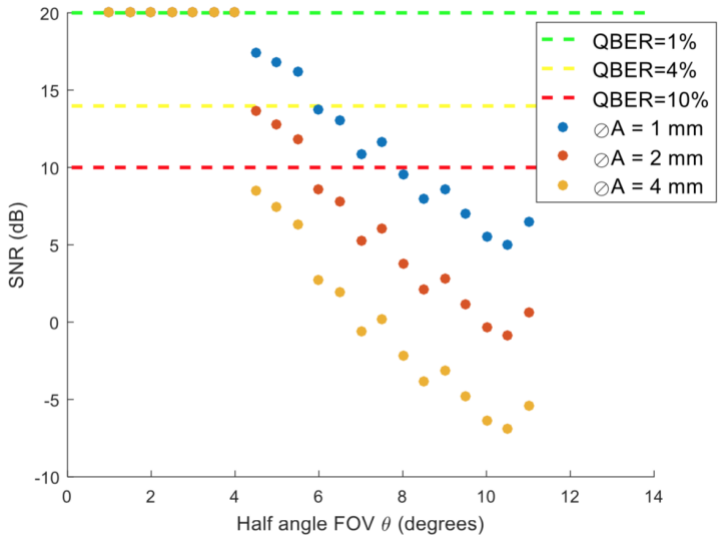

Fig. 13. SNR with filtered experimental ambient light vs half angle FOV

IX. Conclusions

In this paper, a QKD link model was described. The model was simulated for a practical room environment using commercial product parameters for the transmitter and receiver. The simulation used the water and carbon dioxide absorption band between 1360 – 1370 nm of the ASTM spectrum to mitigate ambient light. For each half angle FOV θ, a spectral filter bandwidth was designed to compensate for the spectral filter passband shift. Thus, the ambient light has more effect on the SNR at increasing half angle FOV θ. The results of the simulation determined that varying Airy disk diameters will provide more link loss which affect the SNR and reduce the half angle FOV θ. The simulation can use up to 4 mm Airy disk diameters to operate an SNR above QBER = 10%. An experiment was conducted to obtain measured ambient light data. Results show levels of light several orders of magnitude greater than that simulated. This is caused by the Spectrogon filter not reducing the light outside of the narrow bandwidth enough. The simulation results showed that the QKD link is feasible up to 5.5 degrees using a 1 mm Airy disk diameter for a target QBER = 4% using the experimental data.

X. References

[1] D. R. Myers *et al.*, *NREL Spectral Standards Development and Broadband Radiometric Calibrations* (Conference: Presented at the National Center for Photovoltaics and Solar Program Review Meeting, 24-26 March 2003, Denver, Colorado.). ; National Renewable Energy Lab. (NREL), Golden, CO (United States), 2003, pp. Medium: ED; Size: 6 pp. 1-3.

[2] H. Chun *et al.*, "Handheld free space quantum key distribution with dynamic motion compensation," *optics express*, vol. 25, no. 6, pp. 6784-6795, 2017.

[3] W. T. Buttler *et al.*, "Free-space quantum-key distribution," *Physical Review A*, vol. 57, no. 4, pp. 2379-2382, 04/01/1998 1998.

[4] W. T. Buttler *et al.*, "Practical free-space quantum key distribution over 1 km," *Physical Review Letters*, vol. 81, no. 15, p. 3283, 1998.

[5] R. J. Hughes *et al.*, "Practical quantum cryptography for secure free-space communications," *arXiv preprint quant-ph/9905009*, 1999.

[6] R. J. Hughes *et al.*, "Practical Free-Space Quantum Cryptography," 1999. University of California, Los Alamos National Laboratory

[7] R. J. Hughes, J. E. Nordholt, D. Derkacs, and C. G. Peterson, "Practical free-space quantum key distribution over 10 km in daylight and at night," *New journal of physics*, vol. 4, no. 1, p. 43, 2002.

[8] B. Jacobs and J. Franson, "Quantum cryptography in free space," *Optics Letters*, vol. 21, no. 22, pp. 1854-1856, 1996.

[9] J. Rarity, P. Tapster, P. Gorman, and P. Knight, "Ground to satellite secure key exchange using quantum cryptography," *New Journal of Physics*, vol. 4, no. 1, p. 82, 2002.

[10] N. Gisin, G. Ribordy, W. Tittel, and H. Zbinden, "Quantum cryptography," *Reviews of modern physics*, vol. 74, no. 1, p. 145, 2002.

[11] C. H. Bennett and G. Brassard, "Quantum cryptography: public key distribution and coin tossing," *Theor. Comput. Sci.*, vol. 560, no. 12, pp. 7-11, 2014.

[12] D. Elkouss, A. Leverrier, R. Alléaume, and J. J. Boutros, "Efficient reconciliation protocol for discrete-variable quantum key distribution," in *2009 IEEE International Symposium on Information Theory*, 2009, pp. 1879-1883: IEEE.

[13] Y. Ding *et al.*, "High-dimensional quantum key distribution based on multicore fiber using silicon photonic integrated circuits," *npj Quantum Information*, vol. 3, no. 1, p. 25, 2017.

[14] I. N. Sokolik, "Absorption by atmospheric gases in the IR, visible and UV spectral regions," *School of Earth and Atmospheric Sciences, Georgia Institute of Technology [Online]. Available: http://irina.eas.gatech.edu/EAS8803_Fall2009/Lec6.pdf*, 2009.

[15] S. M. Sze and K. K. Ng, *Physics of Semiconductor Devices*, 3rd ed. Hoboken, New Jersey: John Wiley & Sons, Inc., 2007, pp. 663-742.

[16] Laser Components, "Silicon Geiger Mode Avalanche Photodiode," April 2016. Accessed on: 30 October 2017 [Online]. Available: https://www.lasercomponents.com/fileadmin/user_upload/home/Datasheets/lcd/sap-series.pdf

[17] ID Quantique, "Redefining Measurement. ID120 Visible Single-Photon Detector," May 2017. Accessed on: 30 October 2017 [Online]. Available: https://marketing.idquantique.com/acton/attachment/11868/f-0238/1/-/-/-/-/ID120_Brochure.pdf
[18] Laser Components, "Single Photon Counting Module COUNT-Series," July 2017. Accessed on: 30 October 2017 [Online]. Available: https://www.lasercomponents.com/fileadmin/user_upload/home/Datasheets/lcp/count-series.pdf
[19] Excelitas Technologies, "SPCM-AQRH Single Photon Counting Module," Accessed on: 30 October 2017 [Online]. Available: http://www.excelitas.com/Downloads/DTS_SPCM-AQRH.pdf
[20] E. Hecht, *Optics*. Harlow: Pearson Education Limited, 2017.
[21] Semrock, "Filter Spectra at Non-normal Angles of Incidence," *IDEX Health & Science LLC*, 2019. Accessed on: 23 February 2019 [Online]. Available: https://www.semrock.com/filter-spectra-at-non-normal-angles-of-incidence.aspx
[22] Edmund Optics Worldwide, "Compound Parabolic Concentrators (CPCs)," 2019. Accessed on: 20 February 2019 [Online]. Available: https://www.edmundoptics.com/f/compound-parabolic-concentrators-cpcs-3213/13944/
[23] R. Boyd, *Radiometry and the Detection of Optical Radiation*. New York: John Wiley & Sons, Inc., 1983.
[24] Micro Photon Devices, "InGaAs SPAD - freerunning," June 2014. Accessed on: 20 February 2019 [Online]. Available: http://www.micro-photon-devices.com/Docs/Datasheet/InGaAs_Datasheet_freerunning.pdf
[25] Spectrogon, "Narrow Bandpass Filters," 22 March 2018. Accessed on: 24 February 2019 [Online]. Available: https://www.spectrogon.com/wp-content/uploads/spectrogon/NB-1370-010-nm.pdf